Fifth International Conference on CFD in the Process Industries
CSIRO, Melbourne, Australia
13-15 December 2006

FLUID FLOW, HEAT TRANSFER AND INCLUSION MOTION IN MOLTEN STEEL CONTINUOUS CASTING TUNDISHES

Lifeng ZHANG

Professor, Dept. of Materials Science & Engineering, Norwegian University of Science & Technology (NTNU)
Alfred Getz vei 2, N-7491 Trondheim, Norway, Email: lifeng.zhang@material.ntnu.no
http://www.nt.ntnu.no/users/lifengz/

ABSTRACT

The κ-ε two-equation model is used to simulate the fluid flow in the continuous casting tundish coupling with the effect of thermal buoyancy. The maximum temperature difference in the whole tundish is 8.2 K. The existence of the stopper rod has a big effect on the fluid flow entering the Submerged Entry Nozzle (SEN) and the mold. For the trajectory calculation of inclusions, the Stochastic model yields more accurate inclusion motion than the non-Stochastic model. The average residence time of inclusions decreases with increasing size. The thermal buoyancy favors inclusions removal especially the small inclusions. Using solute transport like the dye injection in water model and copper addition in the real steel tundish cannot accurately study the motion of the inclusions. In the simulation, more than 68% inclusions bigger than 10μm are removed to the top, and less than 32% enters the mold which is larger than the industrial measurement. For inclusions bigger than 100 μm, the effect of thermal buoyancy on their motion can be ignored compared to the inertial buoyancy effect.

INTRODUCTION

The continuous casting tundish serves as a buffer and links the discontinuous process of the secondary metallurgy in the ladle with the continuous casting process in the mold. With continuing emphasis on superior steel quality, it is now increasingly clear that a continuous casting tundish has a far more important function as a continuous reactor than originally envisaged. A modern day steelmaking tundish is designed to provide maximum opportunity for carrying out various metallurgical operations such as inclusion separation, flotation, alloying, inclusion modification by calcium treatment, superheat control, thermal and composition homogenization, leading to the development of a separate area of secondary refining of steel, referred to as "Tundish Metallurgy".

Though some researchers investigated the steel cleanliness in the tundish through industrial trials [1-6], the operation conditions in steel plants, such as the high temperature, the visual opacity of the molten steel, and the massive size of industrial tundishes, hint serious problems for any direct and elaborate industrial experimental investigations of the fluid flow phenomena in tundishes. On the other hand, though the kinematic viscosity of steel is almost equal to that of water, the fluid flow study through water models [5, 7-20] also need to be further proved before using to industrial designs due to the following unclear issues:

- The big difference of the surface tension between the steel (σ_{steel}=1.89 N/m) and the water (σ_{water}=0.073 N/m), affecting the inclusion behavior very much;
- Some similarity criterions are used such as Froude number similarity, Reynolds number similarity, Weber number similarity etc. Sometimes, it is impossible to simultaneously satisfy all of the similarity criterions, but this is vitally important to let the water model results represent those in the real steel system.

Consequently, the numerical simulation becomes a reasonable alternative to investigate the metal flow in the tundish and to design the tundish [21-25]. The numerical simulations of the hydrodynamic phenomena in tundishes include the single phase turbulent fluid flow, multiphase fluid flow if gas injected from ladle shroud or tundish soft-bubbling, residence time distribution, inclusion growth, motion and removal, mixing and grade transition, thermal energy transport, or vortexing formation at the start and the end of casting. Flow optimization in the tundish can be achieved through the tundish shape, and flow control devices such as turbulence inhibitors, impact pads, baffles, weirs and dams. Each tundish is designed in a way as to realize an optimal flow and therefore higher cleanliness of the steel by providing ①high average residence time, ② small severe turbulence, dead and short-circuit volumes, ③ large volume of laminar flow region, ④ forced coagulation in suitable turbulent zones and floating of inclusions, assimilated by cover slag, ⑤avoiding "open (red) eye" creating uncovered surface of molten steel against air absorption.

Heat loss and its associated influence on the fluid flow, residence time, temperature stratification, etc. in continuous casting tundish have been the subject of a large number of mathematical modeling investigations [21, 22, 24]. The conservation equation of the thermal energy has been coupled to the flow equations, incorporating Boussinesque's term ($\rho g \beta \Delta T$) into the momentum balance equation at vertical direction. This is so since the value of Gr/Re^2 in the tundish systems has been known to be much greater than unity. This essentially implies that the effect of the thermal buoyancy (the natural convection) in tundishes is important in the calculation of flow fields.

Understanding the behavior of nonmetallic inclusions in the continuous casting process is important to cope with quality problems such as blisters in ultra-low carbon coils and inclusion defects in heavy plates. In the tundish, the inclusion sources are: deoxidation products, ladle lining erosion product and entrainment of ladle slag (including

reoxidation products by SiO_2, FeO and MnO in slag) carried over from the ladle; entrainment of the tundish slag by the excessive top surface level fluctuation especially at the inlet zone; reoxidation by air in tundish; precipitation of inclusions at lower temperature, such as TiO_2 inclusions; erosion of the tundish lining.

On the other hand, inclusions can be removed by following mechanisms: buoyancy rising and absorption to the top slag; fluid flow transport; argon gas bubble flotation; inclusion growth by collision and Ostwald-Ripening and floation; inclusion absorption to lining refractories.

The final inclusion destination includes the top slag, the lining (safe removal) and mold (possible defects in slab if not be removed in the mold).

The purpose of fluid flow optimization in the tundish is to achieve the best flow pattern to remove inclusions from the molten steel. Hence it is more important to predict the inclusion motion in the tundish than the fluid flow simulation itself. Two main approaches have been applied to model the behavior of inclusions in the molten steel in the tundish: the simple convective-diffusion approach [26-29] and the full trajectory calculations [29].

In the current paper, the simulation of fluid flow and inclusion motion in a 60 t continuous casting tundish is reported, and the effect of the thermal buoyancy on the flow pattern and inclusion motion in the tundish is discussed. The fluid flow near the stopper rod and the SEN outlet are detailed.

MATHEMATICAL FORMULATIONS

Fluid Flow

A typical three dimensional fluid flow model is based on the continuity equation and Reynolds-averaged Navier-Stokes equations for incompressible Newtonian fluids, conserving mass (one equation) and momentum (three equations) at every point in a computational domain [30]. For a steady flow, these equations can be expressed by Eqn.(1) and Eqn.(2).

$$\frac{\partial}{\partial x_i}(\rho u_i)=0 \tag{1}$$

$$\frac{\partial}{\partial x_i}(\rho u_i u_j)=-\frac{\partial P}{\partial x_i}+\frac{\partial}{\partial x_i}\left[\mu_{\text{eff}}\left(\frac{\partial u_i}{\partial x_j}+\frac{\partial u_j}{\partial x_i}\right)\right]+\beta(T_o-T)\rho g_i \tag{2}$$

where ρ is liquid density, (kg·m^{-3}); u_i is velocity component in x_i direction, (m·s^{-1}); x_i is coordinate direction x, y or z, m; P is pressure field, (N·m^{-2}); μ_{eff} is effective viscosity, (kg·m^{-1}·s^{-1}), $\mu_{\text{eff}}=\mu_o+\mu_t$; μ_o is laminar viscosity, (kg·m^{-1}·s^{-1}); μ_t is turbulence viscosity, (kg·m^{-1}·s^{-1}); g_j is magnitude of gravity in j direction, (m·s^{-2}); i, j are coordinate direction indices; β is thermal expansion coefficient of the molten steel, K^{-1}; T is temperature of the molten steel, K; T_o is the temperature at inlet, K.

The κ-ε model gives the turbulent viscosity as

$$\mu_t=\rho C_\mu\frac{\kappa^2}{\varepsilon} \tag{3}$$

where C_μ= 0.09; κ is turbulent kinetic energy, (m^2·s^{-2}); ε is turbulent dissipation, (m^2·s^{-3}).

This approach requires solving two additional partial differential equations for the transport of turbulent kinetic energy and its dissipation rate.

$$\rho u_j\frac{\partial\kappa}{\partial x_j}=\frac{\partial}{\partial x_j}\left(\frac{\mu_t}{\sigma_\kappa}\frac{\partial\kappa}{\partial x_j}\right)+\mu_t\frac{\partial u_j}{\partial x_i}\left(\frac{\partial u_i}{\partial x_j}+\frac{\partial u_j}{\partial x_i}\right)-\rho\varepsilon \tag{4}$$

$$\rho u_j\frac{\partial\varepsilon}{\partial x_j}=\frac{\partial}{\partial x_j}\left(\frac{\mu_t}{\sigma_\varepsilon}\frac{\partial\varepsilon}{\partial x_j}\right)+C_1\mu_t\frac{\varepsilon}{\kappa}\frac{\partial u_j}{\partial x_i}\left(\frac{\partial u_i}{\partial x_j}+\frac{\partial u_j}{\partial x_i}\right)-C_2\frac{\varepsilon}{\kappa}\rho\varepsilon \tag{5}$$

where σ_κ, σ_ε, C_1, C_2 are empirical constants, and σ_κ=1.0, σ_ε=1.3, C_1=1.44, C_2=1.92.

This approach needs special “wall functions” as boundary conditions in order to achieve reasonable accuracy on a coarse grid.

The heat-transfer model solves a 3-D energy transport equation

$$\frac{\partial(\rho u_i h)}{\partial x_i}=\frac{\partial}{\partial x_i}\left(k_{\text{eff}}\frac{\partial T}{\partial x_i}\right) \tag{6}$$

where h is enthalpy in J·kg^{-1} and k_{eff} is effective thermal conductivity in W·m^{-1}·K^{-1}, controlled mainly by the turbulence model.

$$k_{\text{eff}}=k_o+\frac{c_P\mu_t}{Pr_t} \tag{7}$$

where Pr_t is energy Prandtl number, Pr_t=0.85; k_o is laminar thermal conductivity, W·m^{-1}·K^{-1}; c_P is specific heat in J·kg^{-1}·K^{-1}.

Inclusion Motion

Inclusions trajectories can be calculated using the Langrangian particle tracking method, which solves a transport equation for each inclusion as it travels through a previously calculated velocity field. To obtain significant statistics, the trajectories of several thousand individual inclusions should be calculated, using different starting points. The trajectory of each inclusion can then be calculated incrementally by integrating its local velocity as Eqn.(1).

$$\frac{\mathrm{d}l_{pi}}{\mathrm{d}t}=u_{pi} \tag{8}$$

where l_{pi} is inclusion location at any time, m.

The inclusion velocity equation can be derived from the force balance. Here the drag force, F_d, and the gravitational force, F_g, are considered. Thus the total force acting on the inclusion, F, is represented by

$$F=m_p a_p=m_p\frac{\mathrm{d}u_p}{\mathrm{d}t}=F_d+F_g=\frac{\pi}{8}d_p^2\rho C_D(u_p-u)^2-\frac{\pi}{6}d_p^3 g(\rho-\rho_p), \tag{9}$$

which yields the following inclusion velocity equation

$$\frac{\mathrm{d}u_{pi}}{\mathrm{d}t}=\frac{3}{4}\frac{1}{d_p}\frac{\rho}{\rho_p}C_D(u_{pi}-u_i)^2-\frac{(\rho-\rho_p)}{\rho_p}g_i \tag{10}$$

where m_p is particle mass; a_p is particle acceleration rate; u is known liquid velocity; ρ is inclusion and liquid densities, kg·m^{-3}; g is gravity acceleration, 9.8 m/s^2 along the vertical directions and zero at other directions; C_D is drag coefficient as a function of inclusion Reynolds number, given by

$$C_D=\frac{24}{Re_p}\left(1+0.186Re_p^{0.653}\right) \tag{11}$$

.

The effect of the turbulent fluctuation on the motion of inclusions can be modeled crudely from a κ-ε flow field by adding a random velocity fluctuation at each step, whose magnitude varies with the local turbulent kinetic energy level. Here, two models are compared to investigate the effect of the turbulent fluctuation on the motion of inclusions:

Non-Stochastic model: The instantaneous fluid velocity is the time average fluid flow velocity,

$$u = \overline{u} \tag{12}$$

Stochastic model: The instantaneous fluid velocity can be represented by

$$u = \overline{u} + u' = \overline{u} + \xi\sqrt{2k/3}\,, \tag{13}$$

where u is instantaneous fluid velocity, m/s; $\overline{u}$ is average fluid phase velocity, m/s; u' is random velocity fluctuation, m/s. This is the so-called random walk model. In this model, the inclusion interacts with fluid phase turbulent eddies over the eddy lifetime. When the eddy lifetime is reached, a new value of the fluid instantaneous velocity is obtained by applying a new value of random number ξ. Each eddy is characterized by a Gaussian distributed random velocity fluctuation u', keeping constant over the characteristic lifetime of the eddies and a lifetime scale τ_e. The expression of the life time scale of the eddy, τ_e, is as follows

$$\tau_e = 2C_L\,\kappa/\varepsilon \tag{14}$$

where C_L =0.15.

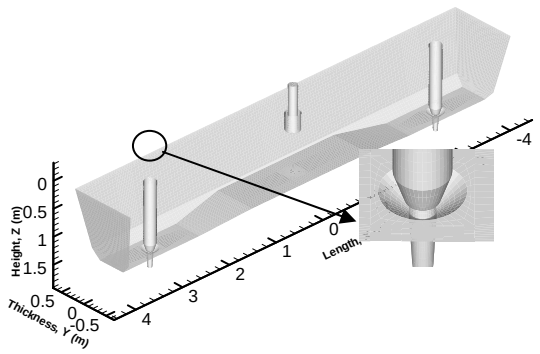

Figure 1. Geometry and dimensions of tundish

PARAMETERS AND BOUNDARY CONDITIONS

Fig.1 and Table 1 show the dimensions, parameters and boundary conditions of the tundish, as reported in Ref. [23], and the average size of the cells should be smaller than 30 mm. The total cells in the tundish mesh system to be studied is 305 080, and the average size of the cells is around 30.1 mm. The first wall-adjacent grid size is estimated to be 1 mm using the method recommended by ZHANG [23]. The QUICK discretization scheme is used. The relaxation factors are 0.3, 0.7, 0.8 and 1.0 for pressure, momentum, turbulence energy and its dissipation, and heat transfer respectively. During iteration, the convergence is assumed to reach that all the normalized un-scaled residuals [23] are smaller than 10^{-5}. The density of inclusions is 5 000 kg/m^3, which is far larger than that of pure alumina (3 000 kg/m^3). This is to account for the molten steel moving together with the alumina cluster and to comprise the simplification of spherical inclusions but not clusters, as suggested by Mike et al [29]. 7 000 inclusions (50 trials to model the effect of Random Walk, 140 inclusions each trial) are injected into the tundish through the inlet. As boundary conditions for inclusion motion, the inclusions are assumed to escape once touching the top surface and outlets of the tundish, and inclusions are assumed to be reflected at other walls. Different size inclusions are investigated, such as 10 μm, 50 μm, 100 μm, 200 μm and 300 μm. To obtain the residence time of the molten steel, the trajectory of solute particles, which have the same density as the molten steel (7 020 kg/m^3) so no inertial buoyancy during their motion, are calculated.

Parameter	Data
Tundish capacity	8.92 m^3
Distance between two outlet	6 100 m
Depth of molten steel	1.20 m
Inclination angle of long wall	9°
Inclination angle of short wall	11.5°
Submergence depth of ladle shroud	300 mm
Inner diameter of ladle shroud	150 mm
Outer diameter of ladle shroud	250 mm
Diameter of well at bottom of tundish	300 mm
Height of well at bottom of tundish	85 mm
Upper diameter of upper nozzle of SEN	95 mm
Under diameter of upper nozzle of SEN	70 mm
Length of upper nozzle of SEN	248 mm
Diameter of stopper rod	200 mm
Depth of stopper rod to well	65 mm
Casting speed	1.2 m·min^{-1}
Slab section	1 300 mm×250 mm
Density of molten steel	7 020 kg·m^{-3}
Laminar viscosity of molten steel	0.006 7 kg·m^{-1}·s^{-1}
Molecular weight of molten steel	55.85 kg·kg^{-1}·mol^{-1}
Parameter	Data
Reference temperature	1 823 K
Reference density of molten steel	7 020 kg·m^{-3}
Inlet velocity	0.736 m·s^{-1}
Inlet turbulent energy	0.002 565 m^2·s^{-2}
Inlet turbulent energy dissipation rate	0.009 626 m^2·s^{-3}
Inlet temperature	1 853 K
Outlet condition	Pressure outlet
Specific heat [31]	750 J·kg^{-1}·K^{-1}
Thermal conductivity [31]	41 W·m^{-1}·K^{-1}
Thermal expansion coefficient	1.0 ×10^{-4} K^{-1}
Heat flux at free surface [31]	15 kW·m^{-2}
Heat loss from bottom wall [31]	1.4 kW·m^{-2}
Heat loss from long wall [31]	3.2 kW·m^{-2}
Heat loss from short wall [31]	3.8 kW·m^{-2}
Heat loss from bottom wall [31]	1.4 kW·m^{-2}
Heat loss from internal walls (dam, weir, stopper rod) [31]	1.75 kW·m^{-2}
Thickness of wall refractory	0.2 m
Thickness of top slag	0.05 m
Thermal conductivity of refractory[23]	1.5 W·m^{-1}·K^{-1}
Heat capacity of lining refractory [32]	1 260 J·kg^{-1}·K^{-1}

Table 1 Parameters and boundary conditions used in simulation

RESULTS AND DISCUSSIONS: FLUID FLOW

The fluid flow pattern of the molten steel on the central face in the tundish in x direction is shown in Fig.2. The main difference of the velocities between isothermal and non-isothermal simulations is at the circled area in the

figure, where the fluid flow tend upwards in the non-isothermal simulation which is induced by the thermal buoyancy effect.

Though there are no flow control devices in the tundish, there is no short circuit flow between the inlet and the outlet at steady fluid flow process, and the molten steel even flows back to the inlet near the bottom of the outlet region, which can be clearly seen from the velocity vector distribution at the bottom of the tundish (Fig.3). The possible reasons for this phenomenon are that the long distance (3.05 m) between inlet and outlet weakens the strong momentum of the inlet stream and the non-flat bottom may lead to the fluid flow a little upward. The flat bottom of the tundish is assumed in many literatures. However, just like in 1987, He et al [11] revealed the importance of the wall inclination on the fluid flow pattern in the tundish, and the non-flat bottom may also affect the fluid flow in the tundish very much.

It should be emphasized that at the start of casting (transient state period), there may be a short circuit flow from inlet to outlet when the height of molten steel in tundish is small.

The main difference of the flow pattern along the walls between the isothermal and non-isothermal simulation at the place with circles is shown in Fig.4. The upward flow along the long wall is observed only in the non-isothermal simulations. Fig.4 also shows that the thermal buoyancy has little effect on the fluid flow in the inlet zone.

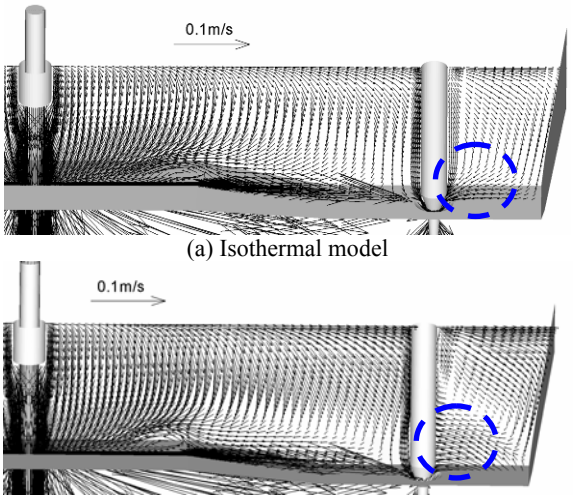

(a) Isothermal model

(b) Non-isothermal model

Figure 2. Velocity vector distribution at longitudinal center face of tundish

The molten steel firstly impinges the bottom of the tundish, and flows upward but tends to the outlet along the long wall near the inlet, reaches the top surface, then flows towards the outlet zone on the top, and then flows downwards along the short wall, reaches the outlet and then flows towards the inlet at the bottom. Fig.4 is the iso-surface with x velocity of 0 m/s (longitudinal direction) of the molten steel in the tundish, which shows that only in the region below the top surface and above the bottom of the inlet zone, the molten steel flows from the inlet to the outlet. In other regions, like the inside of the dark part in the Fig.4, the molten steel backs to the inlet from the outlet. There are two ridges generated in the tundish.

Fig.5 is the distribution of velocity vectors and viscosity ratio ($TU=\mu_t/\mu_0$) on some section of the non-isothermal tundish. The inlet zone has larger turbulent viscosity than other place. On the top, the flow is always from the inlet to outlet, which is opposite to the bottom of the outlet zone. The maximum viscosity in the tundish is 700 times larger than the laminar viscosity, which indicates the strong turbulence flow in the tundish.

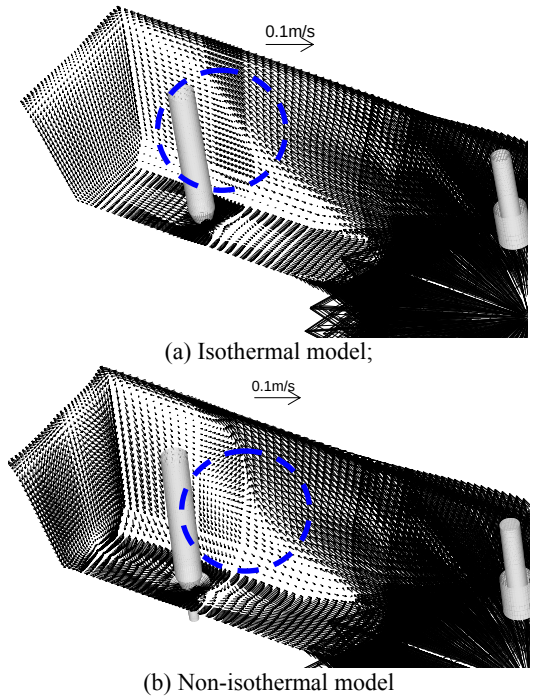

(a) Isothermal model;

(b) Non-isothermal model

Fig.ure 3. Velocity vector distribution along long wall, short wall and bottom of tundish

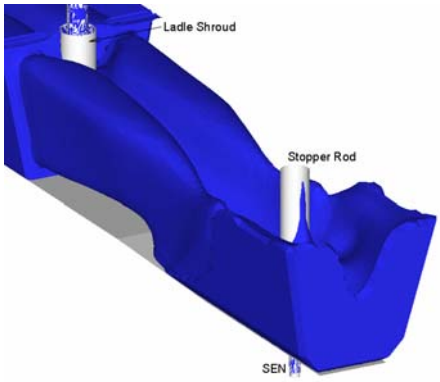

Figure. 4. Iso-surface with x velocity of 0 m/s (longitudinal direction) of molten steel in non-isothermal tundish

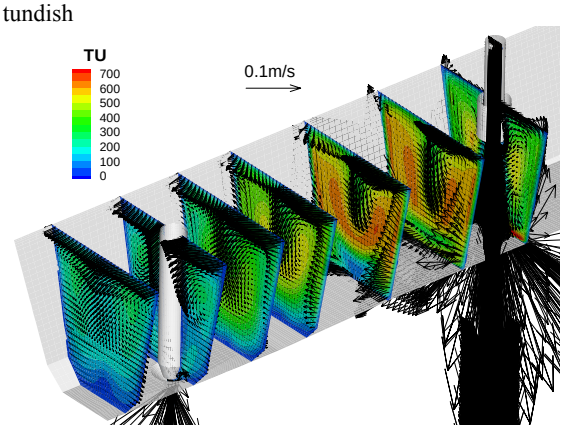

Figure 5. Distribution of velocities and viscosity ratio (TU) on some section of tundish

The temperature difference between inlet and outlet is 3−4 K, as shown in Fig.6, but there is much lower temperature in some regions but not at the outlet, and the maximum temperature difference is 8.2 K. The temperature near the stopper rod and the short wall are obviously lower than that in the inlet zone (Fig.7). The effect of round ladle shroud on temperature distribution is also shown in Fig.7, which indicates a curved (round) temperature contour on the bottom and long walls, also in the bulk of the tundish. Many literatures ignore the effect of the shape of the ladle shroud on the flow in the tundish by assuming a rectangular inlet, which will not yield the round contour as the current simulation, therefore will induce some error for the fluid flow in the tundish.

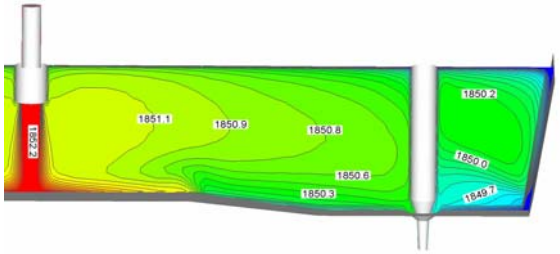

Figure 6. Temperature distribution at longitudinal center face of tundish

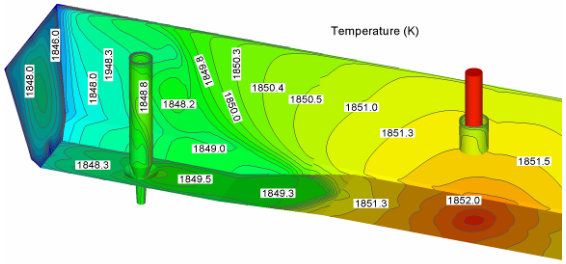

Figure 7. Temperature distribution on long wall, short wall and bottom of tundish

The temperature contour on the wall of the stopper rod and the tundish walls near the rod is shown in Fig.8, in which the left side of the stopper rod is the short wall. The temperature difference is 1 K on the surface of the stopper rod. And the right hand side is with higher temperature due to the incoming flow near the top surface. After impinging on the right hand surface of the stopper rod, the molten steel flows downward to the outlet along the surface, as shown in Fig.9, therefore there is a high temperature stagnant point.

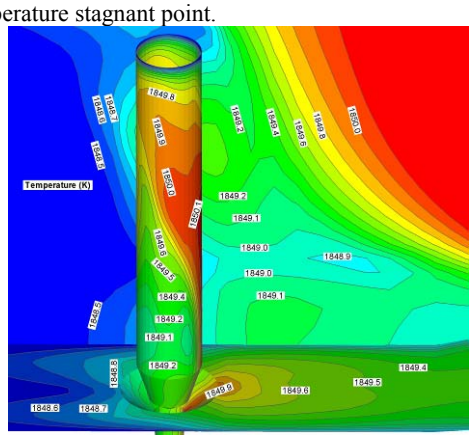

Figure 8. Temperature distribution on stopper rod surface and its near region

The velocity distribution near the wall of the stopper rod of the isothermal tundish is very different from that of the non-isothermal tundish. In the isothermal tundish, the jet impinges on the top part of the stopper rod, and then flows downwards everywhere of its surface. However, in the non-isothermal tundish, the jet impinges on the stopper rod at the top part from the right, but at the lower part, the flow is from left to right with slight upwards at the middle height of the rod and slight downward at the lower part of the rod. This flow pattern has strong effect on the flow entering the well at the bottom of the tundish, through which the molten steel enters SEN and continuous casting mold. In other words, the existence of the stopper rod has a big effect on the fluid flow entering the SEN and the mold. Now it can be summarized that the following characteristics of the tundish should not be ignored in numerical simulation of fluid flow in the tundish: inclination wall (He and Sahai [11] and in the current study), non-flat bottom (in the current study), holes at the bottom of the dam (in another paper of the current author [33]), the existence of stopper rod (in the current study), and the round shape of the SEN, inlet and outlet (in the current paper).

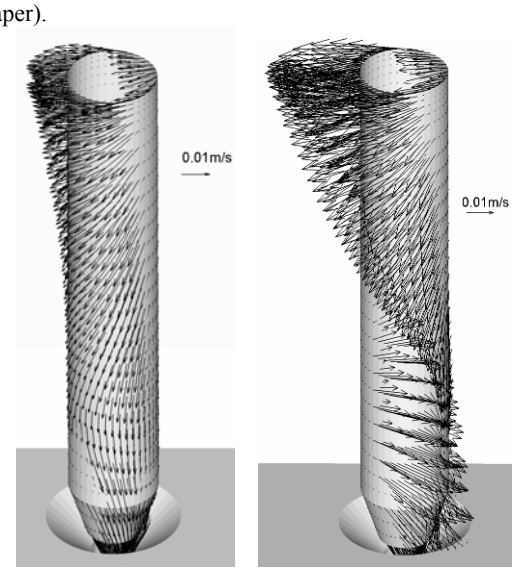

(a) Isothermal model; (b) Non-isothermal model

Figure 9. Velocity vector distribution on stopper rod surface

Fig.10 shows the contours of vertical velocity (z direction), $(v_x^2+v_y^2)^{1/2}$, turbulent energy and its dissipation rate, the static pressure and the temperature entering the well. All of the parameters reveal an asymmetrical distribution. Higher speed is at the side close to the short wall, and larger turbulent energy and its dissipation rate, pressure and temperature are at another side. There is 1 K temperature difference between the two sides of the well. The fluid entering the well surely decides the fluid pattern in the SEN and the continuous casting mold.

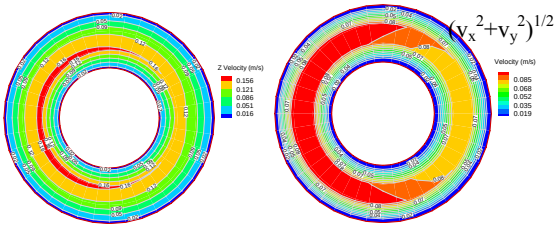

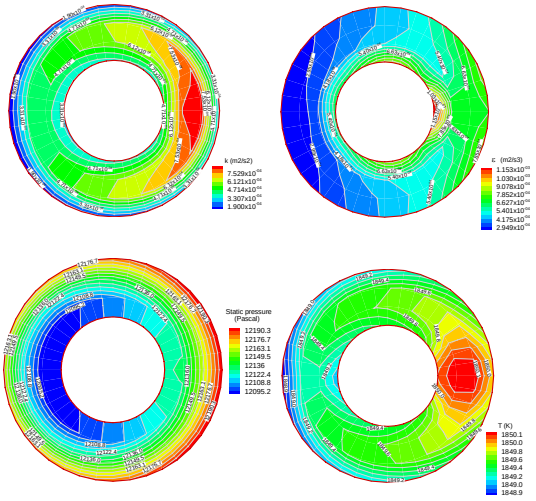

Figure 10. Parameters of stream entering well at bottom of tundish to SEN and mold

Table 2 shows the average value of the flow turbulent energy and its dissipation rate in the tundish. The non-isothermal simulation yields larger value, which indicates again that it is important to couple the natural convection for accurately simulating the fluid flow of the molten steel in the tundish.

	$\kappa/(m^2 \cdot s^{-2})$		$\varepsilon/(m^2 \cdot s^{-3})$	
	Isothermal	Non-Isothermal	Isothermal	Non-Isothermal
Inlet zone	8.3×10^{-4}	9.0×10^{-4}	7.2×10^{-4}	8.0×10^{-4}
Outlet zone	9.4×10^{-5}	1.3×10^{-4}	7.1×10^{-6}	1.2×10^{-5}
SEN	4.0×10^{-3}	3.8×10^{-3}	2.0×10^{-2}	3.3×10^{-2}
Volume average	3.9×10^{-4}	4.4×10^{-4}	3.0×10^{-4}	3.5×10^{-4}

Table 2. Flow pattern in tundish (No flow control)

RESULTS AND DISCUSSION: INCLUSION MOTION

Fig.1 is the typical inclusion trajectories with different size and different models. The effect of random walk can be clearly seen by comparing the shape of the trajectories between the Stochastic and non-Stochastic models. By the Stochastic model, the inclusions move randomly to jump out from the streamline and have more opportunity to touch the top surface to remove from the domain, so their path length is smaller than that by non-Stochastic model. Fig.11 also shows that there is no short circuit path of inclusions directly from the inlet to the outlet, which agrees well with the fluid flow simulation. The final inclusion entrapment positions at the top of the tundish by different models are shown in Fig.12. Obviously the non-Stochastic model is not accurate because by this model, the inclusions can only touch some fixed places of the top [Fig.12 (c) and (d)]. For example, with this model, 300 μm inclusions can only touch the top of the inlet zone to remove [Fig.12 (c)], and the 50 μm inclusion entrapment positions seem stranger, as shown in Fig.12 (d). By the non-Stochastic model, inclusions recirculate more but with regular path, and no obvious upward buoyancy reveals. Inclusions distribute randomly on the whole top with the Stochastic model though larger inclusions more tend to accumulate at the top of the inlet zone such as 300 μm inclusions [Fig.12 (a)]. Large inclusions have larger buoyancy rising velocities (inertial buoyancy), so they are earlier to be removed to the top of the tundish than smaller ones (Fig.11). Smaller inclusions more dispersedly distribute at the whole top because they move within the fluid flow much longer and therefore have more opportunity to reach the top of the outlet zone.

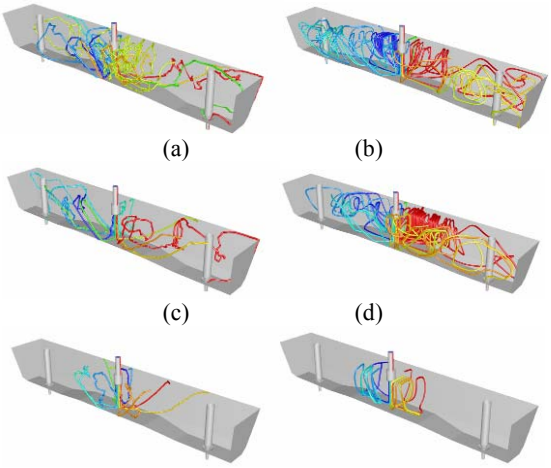

(a) 50 μm, Stochastic model; (b) 50 μm, non-Stochastic model; (c) 100 μm, Stochastic model; (d) 100 μm, non-Stochastic model; (e) 300 μm, Stochastic model; (f) 300 μm, non-Stochastic model

Figure 11. Effect of random walk on the trajectory of 9 inclusions with different sizes in the non-isothermal tundish

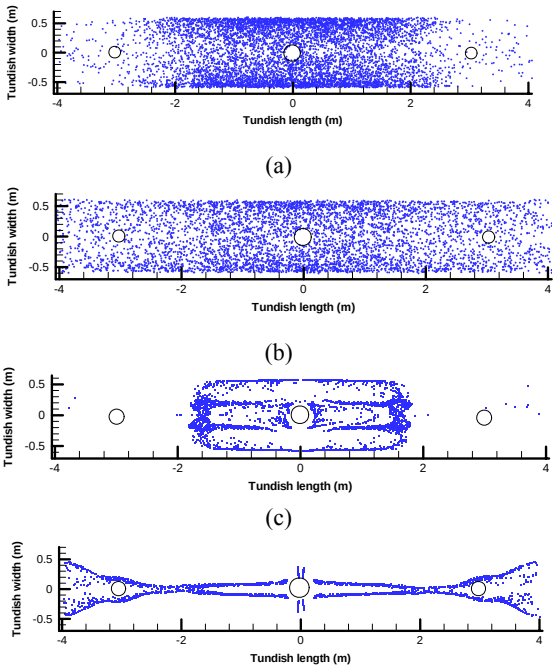

(a) 300 μm, Stochastic model; (b) 50 μm, Stochastic model; (c) 300 μm, non-Stochastic model; (d) 50 μm, non-Stochastic model

Figure 12. Entrapment positions of 7 000 inclusions with different sizes at top surface of tundish

Fig.13 shows the calculated minimum time of inclusions to outlets and the top surface of the tundish. For real inclusions (5 000 kg/m^3), larger inclusions arrive outlets later than smaller inclusions, and reach the top surface earlier than smaller inclusions. The thermal buoyancy leads inclusions, especially those smaller than 200 μm, earlier to out of the domain. For inclusions larger than 200 μm, the effect of inertial buoyancy coming from the density difference between the inclusions and the molten steel becomes stronger than that of the thermal buoyancy. The minimum time to the top and to outlets of solute particles depends little on inclusion size, around 80 s to outlets and 11 s to the top due to no inertial buoyancy for solute particles.

Fig.14 shows the calculated maximum time of inclusions to outlets and the top surface of the tundish. For real inclusions, larger inclusions stay in the tundish shorter than small ones. The thermal buoyancy leads inclusions, especially those smaller than 200 μm, to stay in the tundish shorter than that in the isothermal simulations. For >200 μm inclusions, the inertial buoyancy becomes stronger than the thermal buoyancy, so the latter affects little on their motion though affecting the fluid flow very much. The maximum time to the top and to outlets of solute particles depends little on inclusion size, around 2 000−2 500 s.

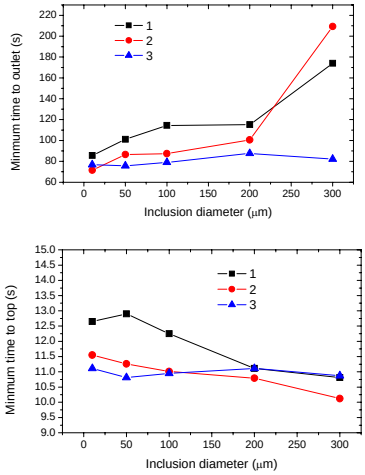

1—Isothermal flow, ρ_p=5 000 kg·m^{-3}; 2—Non-isothermal flow, ρ_p=5 000 kg·m^{-3}; 3—Non-isothermal flow, ρ_p=7 020 kg·m^{-3}

Figure 13. Calculated minimum time of inclusions to outlets and top surface of tundish

Fig.15 is the calculated average residence time of inclusions in the tundish. The average residence time of inclusions decreases with increasing the inclusion size because larger inclusions have bigger buoyancy rising velocity so easier to move to the top. For the non-isothermal simulation, the average residence time of inclusions is smaller than that of isothermal simulation especially for inclusions smaller than 200 μm. This indicates again that the thermal buoyancy favors inclusions removal especially small ones. Fig.15 also shows that the residence time of inclusions is always smaller than that of the solute particles in the non-isothermal simulation.

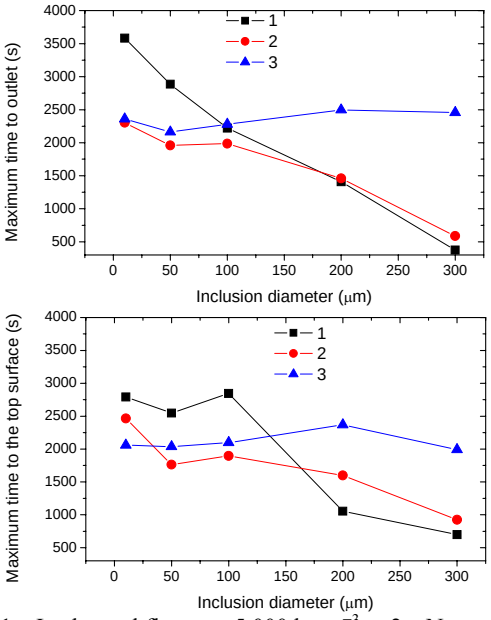

1—Isothermal flow, ρ_p=5 000 kg·m^{-3}; 2—Non-isothermal flow, ρ_p=5 000 kg·m^{-3}; 3—Non-isothermal flow, ρ_p=7 020 kg·m^{-3}

Figure 14. Calculated maximum time of inclusions to outlets and top surface of tundish

The theoretical residence time of the molten steel is around 660 s, which equals to the tundish capacity divided by the flow rate of the molten steel. As shown in Fig.15, if including the effect of random walk and assuming solute particles to be removed out of the domain by touching the top surface, the average residence time of solute particles is only around 255 s, far smaller than the theoretical residence time of the molten steel in the tundish. If ignoring the random walk effect, and assuming inclusions to be reflected when they touching the top surface, and the only destination of inclusions is the outlet (to the mold), the calculated average residence time of the solute particles is 541.5 s, which is more closer to the theoretical residence time.

The minimum residence time, the maximum residence time and the average residence time of solute particles are independent of their sizes. Minimum time is 75 s to outlets and 11 s to the top. Maximum time is 2 300 s to outlets and 2 000 s to the top. The average time is around 250 s. These times for real inclusions greatly varies with sizes. Therefore, using solute transport like the dye injection in the water model or copper addition in the molten steel in the industrial tundish cannot accurately study the motion of inclusions. On the other hand, these times of solute particles can be considered as those of the molten steel due to their same density. So, the residence time of the molten steel is very different from that of inclusions. Investigating the residence time of the molten steel, therefore, is not so meaningful for the motion of inclusions. Hence, to accurately investigate the motion of inclusions, the mathematical simulation on the fluid flow and inclusion motion in the real steel tundish and the water model of non-solute particles are better than the solute transport like the dye injection in the water model or copper addition in the molten steel in the industrial tundish.

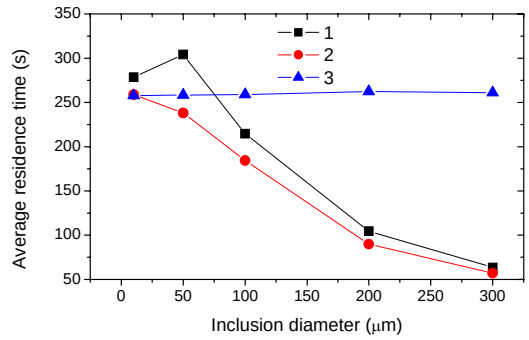

1—Isothermal flow, ρ_p=5 000 kg·m^{-3}; 2—Non-isothermal flow, ρ_p=5 000 kg·m^{-3}; 3—Non-isothermal flow, ρ_p=7 020 kg·m^{-3}

Figure 15. Calculated average residence time of inclusions in tundish

Fig.16 is the typical histogram of the average residence time of 50 μm and 300 μm inclusions in the molten steel. The average residence time is around 240 s for 50 μm inclusions and around 55 s for 300 μm inclusions. Larger inclusions are faster to be removed. Fig.17 is the fractions of inclusions to outlets and the top surface. In the simulation, more than 68% inclusions larger than 10 μm are removed to the top, and less than 32% enters the mold. Almost all of the inclusions larger than 200 μm are removed. In the industrial trial of this 60 t tundish with weirs and dams, inclusions smaller than 50 μm are removed by about 30%, inclusions larger than 50 μm are removed by 51%−74%, and almost all of the inclusions larger than 200 μm are removed in the tundish [34]. The possible reasons for the discrepancy between the simulated and the measured are as follows:

(1) The generation of new inclusions by the reoxidation of melt with the air, slags and lining refractory is ignored in current simulation;

(2) The real density of alumina clusters is possibly larger than 5 000 kg/m^3, causing a smaller buoyancy rising velocity;
(3) The removal criterion in the current simulation is not perfect, because some inclusions may reflect back to the bulk after touching the interface between the molten steel and the slag especially at a very big velocity before touching and some inclusions in top slag may be re-entrained back to the bulk of the steel.

The fractions of solute particles are independent of their size. For inclusions, smaller ones have larger fractions to outlets and smaller fractions to the top. In isothermal simulation, the fractions to outlets are larger and fractions to the top are smaller than that in non-isothermal simulations for inclusions smaller than 100 μm, which hints that the thermal buoyancy favors their removal to the top surface. For inclusions larger than 100 μm, the effect of the inertial buoyancy becomes stronger than that of the thermal buoyancy.

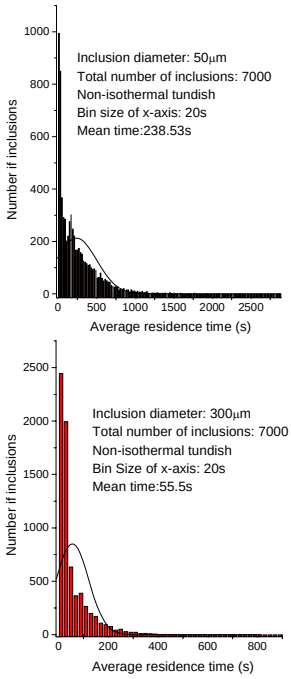

Figure 16. Histogram of average residence time of 50 μm and 300 μm inclusions in molten steel

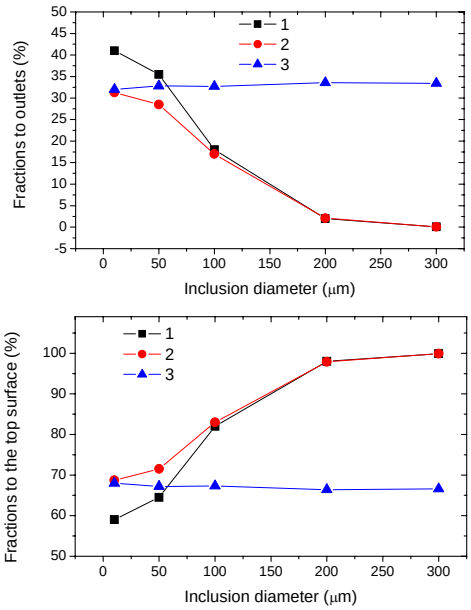

1—Isothermal flow, ρ_p=5 000 kg·m^{-3}; 2—Non-isothermal flow, ρ_p=5 000 kg·m^{-3}; 3—Non-isothermal flow, ρ_p=7 020 kg·m^{-3}

Figure 17. Fractions of inclusions to outlets and top surface of tundish

Not all inclusions with the average residence time smaller than that of the molten steel are removed to the top of the tundish. Some of them still remain in the molten steel and flow into the mold. For examples, the average residence time of 100 μm inclusions is 185 s, far smaller than that of the molten steel (259 s). But there are still 18% of 100 μm inclusions entering the mold. This indicates again that studying the residence time of the molten steel is not full meaningfully for the motion of inclusions.

The thermal buoyancy has no effect on the fraction of inclusions to the top of the inlet zone, as shown in Fig.18, because the thermal buoyancy has little effect on the fluid

flow in the inlet zone, then affects little on inclusion motion in this zone. In inlet zone, though the fluid flow velocity is very high, the inertial buoyancy still influence the motion of inclusions very much, and larger inclusions are removed in the inlet zone more than smaller ones. The thermal buoyancy mainly affects the inclusion motion in the outlet zone and favors the removal of inclusions smaller than 100 μm. For inclusions larger than 100 μm at the outlet zone, the inertial buoyancy becomes more important than the thermal buoyancy, therefore there is little difference between the results of isothermal simulation and non-isothermal simulation.

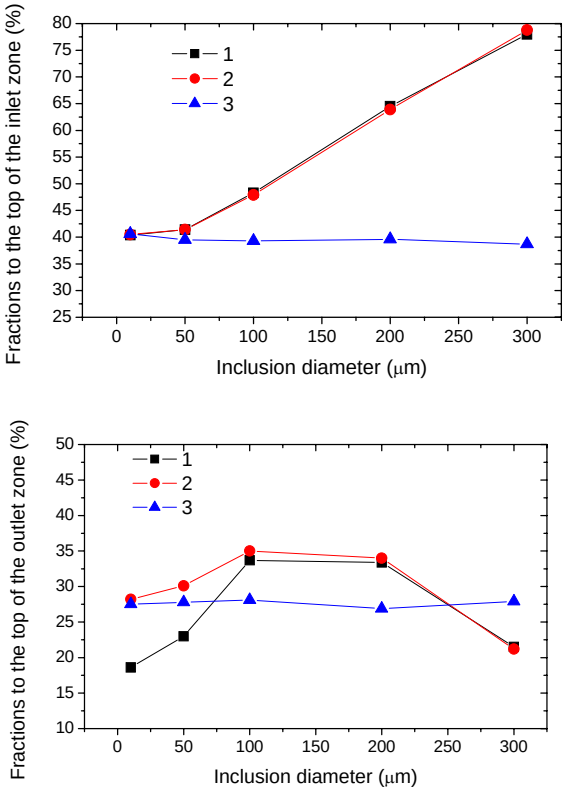

1—Isothermal flow, ρ_p=5 000 kg·m^{-3}; 2—Non-isothermal flow, ρ_p=5 000 kg·m^{-3}; 3—Non-isothermal flow, ρ_p=7 020 kg·m^{-3}

Figure 18. Fractions of inclusions to top of inlet zone and outlet zone

RESULTS AND DISCUSSION: EFFECT OF FLUID CONTROL DEVICES

Steel cleanliness in the 60 tonne two-strand tundish with several flow control devices are compared. The measured removal fractions of >50μm inclusions, T.O., and <50μm inclusions are shown in Fig 19**.** The tundish with one weir and two dams each side achieves the biggest inclusion removal fraction. When use 1 weir and 1 dam each side, the filter on the weir can removal more inclusions. The calculated inclusion removal fraction is shown in Fig.20, which indicates that flow control devices favors the removal of inclusions, especially 50-250μm inclusions. <50μm inclusions almost move with the fluid streamline due to their small Stokes number, and >300μm inclusions are easily removed to the top slag due to their buoyancy rising velocity, even without fluid flow control devices.

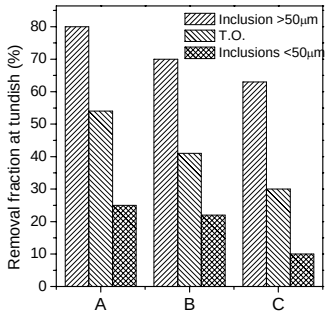

(A: 1 weir with filter and 2 dams each side; B: 1 weir with filter and 1 dam each side; C: 1 weir and 1 dam each side)

Figure 19. Effect of flow control devices on inclusion removal in the 2-strand 60 tonne tundish

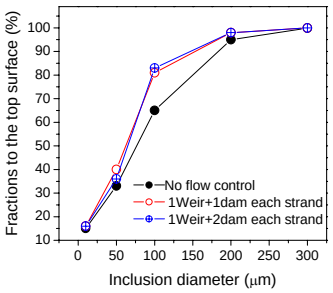

Fig.20 Inclusion removal fraction by numerical simulation

The calculated fluid flow pattern, temperature distribution, and typical inclusion trajectories in tundish without flow control devices and with 1 weir and 1 dam each side are shown in Fig.21 and 22. It should be noticed that in the tundish without flow control devices, there is no short circuit flow between the inlet and the out at the steady state fluid flow process, except at the start period of pouring, and the molten steel even flows back to the inlet near the bottom of the outlet region. The possible reasons include 1). The long distance (3.05m) between the inlet and the outlet weakens the strong momentum of the inlet stream; 2) The non-flat bottom may lead the fluid flow a little upward. The flat bottom simplification is assumed in the fluid flow simulation in many literatures. However, the current simulation indicates that the non-flat bottom affects the fluid flow in the tundish very much. Figure 16 shows that most of 300 μm inclusions touch the top of the inlet zone to remove, and the position of smaller inclusions touching the top are more uniform along the whole top of the tundish without flow control devices, but more closer to the top of the inlet zone in the tundish with 1 weir and 1 dam each side.

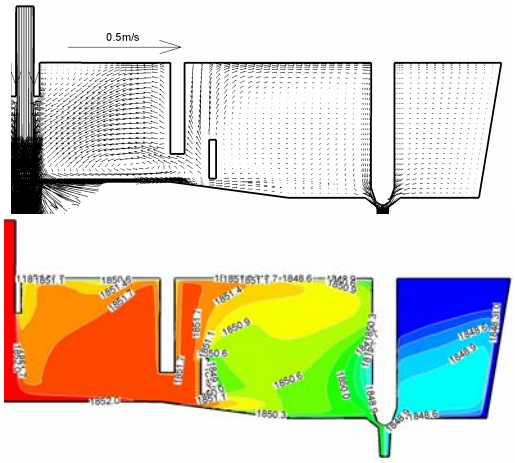

Figure 21. Distribution of velocity vectors and temperature at the longitudinal center face of the tundish with 1 weir and 1 dam each side

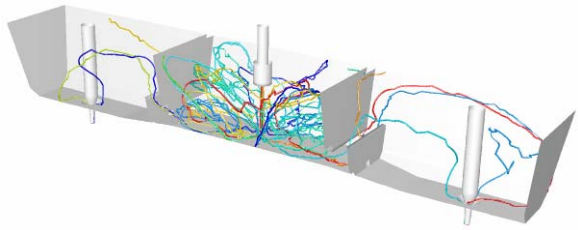

Figure 22. Typical 50μm inclusion trajectories in the 60 tonne continuous casting tundish with 1 weir and 1 dam each side)

CONCLUSIONS

- The natural convection induced by the thermal buoyancy has little effect on the fluid flow in the inlet zone.
- There is no short circuit flow between the inlet and the outlet at the steady fluid flow process.
- The maximum viscosity is 700 times larger than the laminar viscosity due to strong turbulence flow in the tundish.
- The temperature difference between the inlet and outlet is 3−4 K, and the maximum temperature difference in whole tundish is 8.2 K.
- The existence of the stopper rod has a big effect on the fluid flow entering the SEN and the mold.
- The non-isothermal simulation indicates that coupling the natural convection is important to accurately simulate the fluid flow in the tundish.
- The Stochastic model yields more accurate inclusion motion than the non-Stochastic model due to including the effect of the turbulent fluctuation.
- Larger inclusions tend to be entrapped at the top of the inlet zone and smaller inclusions distribute more uniformly at the whole top of the tundish.
- The thermal buoyancy leads inclusions especially those smaller than 200 μm earlier to outlets and the top.
- For inclusions bigger than 100 μm, the inertial buoyancy becomes more important than the thermal buoyancy. Investigating the residence time of the particles in molten steel is not so meaningful for the motion of inclusions.

REFERENCES

1) H. Tanaka, R. Nishihara, I. Kitagawa and R. Tsujino: *ISIJ Internationla*, (1993), **33**(12), 1238.
2) K. Sasai and Y. Mizukami: *ISIJ Int.*, (2000), **40**(1), 40.
3) P. Kovac, J. Jijac, V. Masek, P. Marek, P. Kalmar and K. Michalek: *Metalurgija*, (2003), **42**(4), 249.
4) H. Solhed, L. Jonsson and P. Jonsson: *Metal. & Material Trans. B.*, (2002), **33B**(2), 173.
5) A. Aguilar-Corona, R. D. Morales, M. Diaz-Cruz, J. Palafox-Ramos and H. Rodriguez-Hernandez: *Steel Research*, (2002), **73**(10), 438.
6) H. Solhed and L. Jonsson: *Scand. J. Metallurgy*, (2003), **32**(1), 15.
7) Y. Sahai and T. Emi: *ISIJ Internationla*, (1996), **36**(9), 1166.
8) L. J. Heaslip, A. McLean, D. J. Harris and J. D. Young, in Continuous Casting, **1**, eds., ISS, Warrendale, PA, (1983), 93-112.
9) H.-J. Odenthal, R. Bolling, H. Pfeifer, J.-F. Holzhauser and F.-J. Wahlers: *Steel Research*, (2001), **72**(11+12), 466.
10) G. Wen, L. Zhang, P. Tang, Z. Su, M. Zhu, W. Gu, K. Zhao and G. Song, in ISSTech2003, eds., ISS, Warrandale, PA, (2003), 577-588.
11) Y. He and Y. Sahai: *Metal. Trans B*, (1987), **18B**(2), 81.
12) C. Damle and Y. Sahai: *ISIJ Internationla*, (1996), **36**(6), 681.
13) D. Sheng, C. Kim, J. Yoon and T. Hsiao: *ISIJ Int.*, (1998), **38**(8), 843.
14) J. J. Kim, S. K. Kim, J. W. Kim, S. D. Shim and Y. D. Lee, in 2001 Electric Furnace COnference Proceedings, eds., ISS, Warrandale, PA, (2001), 395-406.
15) H.-J. Odenthal and H. Pfeifer: *Gala Fachtagung-Lasermethoden in der Stromungsmesstechnik*, (2000), 1-7.
16) H.-J. Odenthal, R. Bolling and H. Pfeifer: *2nd Int. COnf. on the Science & Technology of Steelmaking*, (2001), 499-517.
17) H.-J. Odenthal, R. Bolling, H. Pfeifer, J.-F. Holzhauser and F.-J.Wahlers: *4th European Continuous Casting Conference*, (2002), 513-522.
18) H.-J. Odenthal, R. Bolling and H. Pfeifer: *Steel Research*, (2003), **74**(1), 44.
19) H.-J. Odenthal, R. Bolling and H. Pfeifer: *11th Japan-Germany Seminar of Fundamentals of Iron and Steelmaking*, (2002), 86-98.
20) P. K. Jha and S. K. Dash: *ISIJ Internationla*, (2002), **42**(6), 670.
21) L. Zhang: *Journal of Iron and Steel Research International*, (2005), **12**(5), 13.
22) L. Zhang: *Journal of Iron and Steel Research International*, (2005), **12**(4), 20.
23) L. Zhang: *Journal of University of Science and Technology Beijing(English Edition)*, (2005), **12**(116-122),
24) L. Zhang: *Steel Research International*, (2005), **76**(11), 784.
25) L. Zhang and S. Taniguchi: *Metal. & Material Trans. B.*, (2000), **31B**(2), 253.
26) O. J. Ilegbusi and J. Szekely, in Mathematical Modeling of Materials Processing Operations, J. Szekely, L. B. Hales, H. Henein, N. Jarrett, K. Rajamani and I. Samarasekera, eds., The

Metallurgical Society, Warrendale, PA, (1987), 409-429.
27) S. Joo, R. I. L. Guthrie and C. J. Dobson, in Steelmaking Conference Proceedings, **72**, eds., ISS, Warrendale, PA, (1989), 401-408.
28) A. K. Sinha and Y. Sahai: *ISIJ Internationla*, (1993), **33**(5), 556.
29) Y. Miki and B. G. Thomas: *Metall. Mater. Trans. B*, (1999), **30B**(4), 639.
30) J. O. Hinze: *Turbulence*, 2nd ed., eds., McGraw-Hill, New York NY, (1975).
31) S. Chakraborty and Y. Sahai, in The Sixth International Iron and Steel Congress, eds., Nagoya, Japan, (1990), 189-195.
32) V. Panjkovic and J. Truelove: *Second International Conference on CFD in the Mineral and Process Industries*, (1999), 399-404.
33) L. Zhang: *Under preparation to Acta Metallurgica Sinica (English Letters)*, (2005), (I),
34) L. Zhang, B. G. Thomas, K. Cai, L. Zhu and J. Cui, in ISSTech2003, eds., ISS, Warrandale, PA, (2003), 141-156.